JARS Journal of Applied Remote Sensing

RESEARCH PAPER

Mapping aboveground biomass and carbon in salt marshes across the contiguous United States

Anthony D. Campbell[a,b,c,*] **and Lola Fatoyinbo**[a]

[a]NASA Goddard Space Flight Center, Biospheric Sciences Laboratory, Greenbelt, Maryland, United States
[b]Oak Ridge Associated Universities, NASA Postdoctoral Program, Oak Ridge, Tennessee, United States
[c]University of Maryland, Baltimore County, Goddard Earth Sciences Technology and Research II, Baltimore County, Maryland, United States

ABSTRACT. Salt marshes provide extensive ecosystem services, including habitat, recreation, coastal resilience, and carbon sequestration. The United States has the largest extent of mapped salt marshes. Therefore, it is critical to understand the ecosystem's carbon stock and drivers in the contiguous United States (CONUS). Blue carbon ecosystems, including salt marshes, mangroves, and seagrasses, store most of their carbon within the soil; aboveground biomass (AGB) is an important ecosystem indicator. Existing AGB models in salt marshes have medium spatial resolution and limited geographic extent. To improve the spatial resolution to 10 m, we evaluated the use of Sentinel-1 and 2 data for inclusion into the AGB prediction. To incorporate these satellite observations with temporally disparate *in situ* samples, we evaluated the stability of training locations using the Landsat time series, finding that 71% of training data were stable from field sampling to remote sensing observation in 2020. Next, we trained a machine learning regression combining Sentinel-1, Sentinel-2, and Landsat data to predict AGB in salt marshes. We compared model performance with *in situ* testing data between three machine learning algorithms [support-vector machines, random forest, and extreme gradient boosting (XGBoost)], spatial scale (10, 30 m), and training data stability. The best-performing model was the 10 m XGBoost using the stable training data, which achieved a root mean square error of 301.0 and 107.33 at the plot and site scale, respectively. We created an updated 2020 salt marsh extent with Sentinel-1/2, Shuttle Radar Topography Mission, and National Elevation Dataset and estimated 3.6 (3.1 to 4.1) Tg of aboveground carbon across the CONUS. We explored salt marsh biomass drivers and found that the primary drivers of AGB are relative sea level rise, temperature, precipitation, and tidal amplitude. Our results demonstrate the need to monitor these systems to enable management, restoration, and understanding of the ecosystem's resilience to climate change.

Keywords: aboveground biomass; wetlands; blue carbon; machine learning; data fusion; salt marsh

Paper 240165SS received Mar. 12, 2024; revised Aug. 15, 2024; accepted Aug. 29, 2024; published Oct. 1, 2024.

1 Introduction

Salt marsh, mangrove, and seagrass, called blue carbon ecosystems, are critical for addressing climate change.[1] Still, there is significant uncertainty about how changes to these ecosystems impact their carbon stocks in the contiguous United States (CONUS).[2] In the CONUS, 75%

*Address all correspondence to Anthony D. Campbell, anthony.d.campbell@nasa.gov

of blue carbon is found within estuarine emergent wetlands,[3,4] necessitating improved spatial and temporal resolution of carbon monitoring in these ecosystems. Most of these systems' carbon is stored within their soils,[5,6] but aboveground biomass (AGB) is an essential indicator of ecosystem health and changes to the carbon stock. This study utilizes earth observation, data fusion, cloud computing, and machine learning to predict AGB and salt marsh extent. Improved remote sensing monitoring of salt marsh ecosystems is critical for increased ecosystem adoption into nationally determined contributions, identification of restoration sites, and monitoring of restoration outcomes.[7]

Sea level rise (SLR), eutrophication, and storm events drive changes across these systems.[8] The SLR impacts on salt marshes are uncertain, and net change depends on the accommodation space.[9] However, local models predict that an inflection point is rapidly approaching for formerly stable ecosystems with ecosystem-wide change imminent, i.e., replacement of high marsh with low marsh vegetation.[10] Historically, marsh migration has offset losses from sea-level changes.[11] However, marsh migration is not guaranteed in certain landscapes due to vegetation and topography impeding it.[12] In the CONUS, 43% to 48% of coastal wetlands have an accretion deficit and lack space for inland migration.[13] These changes will impact carbon storage.[14] Therefore, a high-resolution repeatable AGB baseline to monitor salt marsh migration is critical to facilitating our understanding of this process's impacts.

The mapping of AGB has a long history within salt marsh environments, with the first studies utilizing Landsat and focusing on predicting the biomass of a single species.[15–17] Since that starting point, a variety of data and platforms have been employed to predict biomass, including unoccupied aerial systems, hyperspectral, LiDAR, and synthetic aperture radar.[18–21] Local studies have demonstrated promising results of Sentinel-2.[18,22–24] Byrd et al.[22] trained a CONUS-wide biomass model, Campbell and Wang[25] demonstrated the training sets applicability outside regions directly surrounding the *in situ* sampling locations, and Woltz et al.[26] created 30 m maps for the CONUS. These studies show the potential and limitations of biomass prediction in salt marsh environments, e.g., training data availability, limited geographic extent of *in situ* samples, and high uncertainty. This study evaluates training data relative to time-series stability to expand the CONUS prediction of AGB to Sentinel-2.

Repeatable mapping methods are necessary to facilitate baseline monitoring. The National Wetland Inventory (NWI), National Oceanic and Atmospheric Administration (NOAA) Coastal Change Analysis Program (C-CAP), and National Land Cover Dataset (NLCD) all have wetland classes that can be used to understand salt marsh change. However, these datasets have limitations. For example, the NWI has infrequent updates for local areas, resulting in a varied mapping date and change estimates for regions.[27] NWI wetland maps can diverge significantly in mapped wetland extent from in situ approaches.[28] C-CAP/NLCD are derived from Landsat, resulting in medium resolution, and NLCD separates salt marshes from other emergent wetlands. The medium spatial resolution can miss fine-scale changes in salt marsh extent, e.g., migration into the upland. The CONUS is frequently a focus of salt marsh research; however, it is seldom considered in its entirety. As the spatial resolution of the data increases, more pixels with a mix of salt marsh, tidal flat, water, and upland exist, making inclusions of non-salt marsh more likely. None of the existing datasets is adequate for tracking change at a fine temporal or spatial scale in salt marsh environments, e.g., interior die-off, storm events, herbivory, restoration, and seasonal variation.

Machine learning methods can provide a robust and accurate prediction of both extent and biomass in blue carbon ecosystems.[29] Random forest is an ensemble decision tree classifier (Breiman 2001[30]). It has been utilized to map mangrove extent and drivers of change,[31] salt marsh biomass,[25] and wetland biomass with high-resolution imagery.[32] XGBoost is more sensitive to parameter tuning and demonstrated improved biomass estimations in tropical forests over random forests.[33] Support vector machine (SVM) is a hyperplane learning algorithm with extensive applications in data science.[34] At the same time, comparisons of machine learning algorithm performance demonstrate the suitability of random forest for blue carbon applications.[29] We explore performance across a subset of algorithms to identify the best for CONUS-wide mapping of salt marsh AGB.

A large uncertainty of salt marsh carbon accounting in the CONUS is marsh extent and change. Previous studies have relied on the NWI, the Soil Survey Geographic Database, and the C-CAP.[2,4] The spatial resolution and revisit time of Sentinel-1 and Sentinel-2 can improve

our ability to track these ecosystems. The suitability of Sentinel-2 is evident when used to map salt marshes in Louisiana with an overall accuracy of >90%[35] and more recent global efforts (Worthington et al. 2024).[36] This study updates the NWI salt marsh extent in all CONUS watersheds to 2020 using Sentinel-1/2 and an ensemble machine learning method to estimate uncertainty. The updated salt marsh extent is used in conjunction with the AGB model estimates to analyze drivers of salt marsh AGB. Because this study predicts biomass at a 10 m resolution with no predictive power outside the marsh environment, a 10-m binary salt marsh classification was conducted and used to constrain the AGB model.

This study seeks to provide insight into carbon monitoring of salt marsh ecosystems by (1) creating a 10-m estimate of AGB within the salt marsh environment, (2) updating salt marsh extent to 2020, and (3) evaluating the drivers of AGB across the CONUS, including SLR, temperature, precipitation, and land cover land use (LCLU). Earth observation and existing *in situ* carbon estimates are combined to provide a spatial prediction of salt marsh carbon stock at a fine spatial resolution for the country with the largest extent of mapped salt marsh.

2 Methods

2.1 Study Area

Recent global mapping of tidal marsh found a third of the global extent to occur within the USA.[36] In the CONUS, salt marshes are composed of a variety of halophytic vegetation, including *Spartina alterniflora*, *Salicornia* spp., *Juncus gerardii*, *Phragmites australis*, *Distichlis spicata*, and *Spartina patens.* Salt marshes are concentrated in the back bays of barrier islands, estuarine bays, and deltas in low-energy environments, allowing for sediment accumulation.[37] In the United States, salt marshes have experienced significant conversion to other land uses, especially in urban areas such as Boston, which is estimated to have lost 81% of its salt marsh extent.[38] Salt marshes can be found across the Atlantic, Pacific, and Gulf coasts of the United States. Salt marsh species vary with tidal amplitude, temperature, salinity, and elevation.

2.2 AGB Modeling

We used Google Earth Engine (GEE) to process the time series data and the MLR package in R statistical software (3.6.2) to train machine learning models to predict AGB.[39] Previous studies found the lack of overlap between Sentinel-1/2 and the *in situ* data collection limited its usefulness in modeling biomass.[18] To address this issue, we identified stable salt marsh pixels, i.e., those that changed little from the biomass sampling year to Sentinel data collection. Stable sampling areas then had the average Sentinel-1 VV, and VH sampled for the 2 weeks preceding and the 2 weeks after the sampled date across the Sentinel-1 archive. We applied the same method to process Sentinel-2 10 m bands and Normalized Difference Vegetation Index (NDVI). A total of 530 samples were deemed stable. Additional biomass samples from the Georgia Coastal Ecosystem Long Term Ecological Research Reserve in 2017 were retrieved from their database and incorporated into the model for 723 stable training points (Fig. 1). We used this subsample to train a 10-m biomass model. We compared the stable model with models trained with all available training locations ($n = 984$). The validation included locations from 2019 for the GCE LTERR [Dataset][40] and sites from Plum Island, MA [Dataset].[41]

Three machine learning algorithms, SVM, extreme gradient boosting (XGBoost), and random forest, were compared with out-of-box cross-validation and *in situ* validation data. Previous studies have demonstrated the potential of this training data[18] for regional[25] and national monitoring of AGB.[26]

2.3 Time Series Stability

We explored the temporal stability of *in situ* training data locations collected before the operation of Senintel-1 and Sentinel-2. We assessed training data stability with a time series analysis of the Soil-Adjusted Vegetation Index. *In situ*, continuous monitoring plots demonstrate significant variation in AGB from 343 to 1324 $g\,m^{-2}\ year^{-1}$ in Plum Island.[42] The biomass plot size ranges from 0.0625 to 1 m^2, much finer than the satellite imagery (10 to 30 m). While fine-scale seasonal variation is minimized at the pixel scale, shifts in vegetation composition or disturbance could cause changes. This study assesses pixel stability using the Landsat archive. *In situ* plots

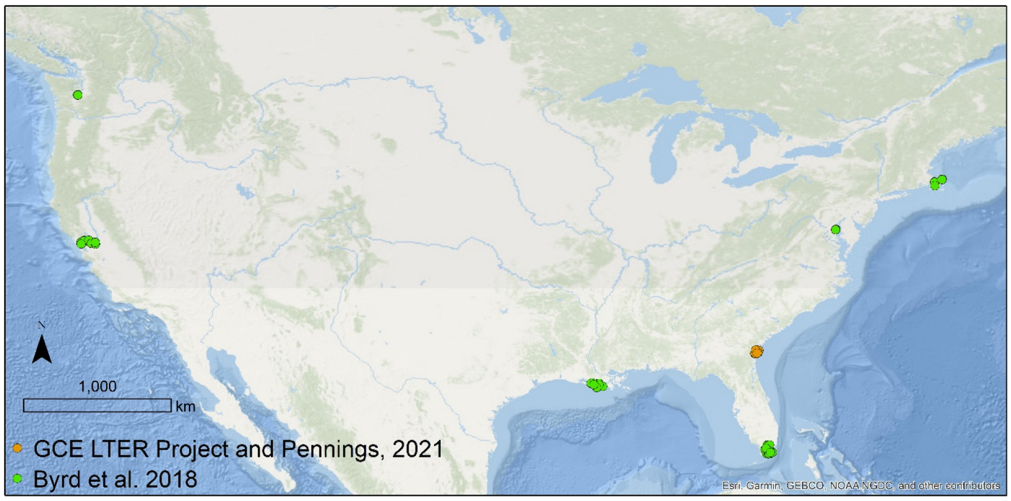

Fig. 1 Model training data and source from either Byrd et al.[18] or GCE LTER Project and Pennings.[40] Service Layer Credits: Esri, Garmin, GEBCO, NOAA NGDC, and other contributors.

collected at the exact location and month were consolidated into a single training point with average biomass and imagery variables. Trend and breakpoints were calculated for the resulting 830 training points. We decomposed the time series using the Prophet package in R, isolating trend and seasonality to determine stability.[43] The training data had many more gain points than losses. Therefore, we derived a change threshold of 0.05 SAVI from the 0.05 quantile of loss. Two hundred sixty-one training locations were outside this threshold, and SAVI increased in 84% of these locations. These excluded points were further analyzed with Breaks for Additive Season and Trend to determine if they had experienced a break following biomass collection (Fig. 2).

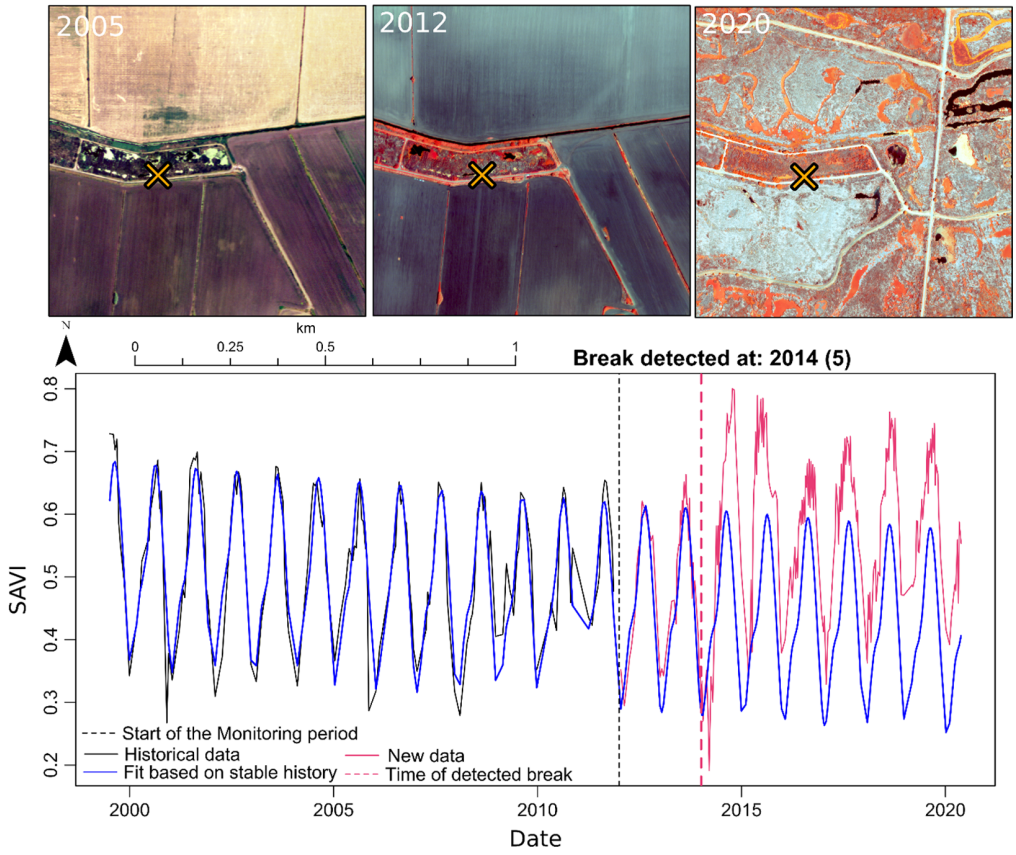

Fig. 2 Stability assessment of a point at Twitchell Island, CA. Time series demonstrates significant divergence from the expectation following biomass field data collection.

The monitoring period was from 1999 to the beginning of the year of sampling. We found that 100% of points with an absolute trend >0.05 also experienced a break. As a final test, we compared models trained with all data and stable training data with two in situ testing sets to verify the performance of this stable training set.

Tides affect salt marshes in various ways and have been addressed in remote sensing research.[25,44,45] The Landsat imagery was tidally filtered using the methods detailed in Campbell and Wang[25] and adapted to GEE. All values were cloud, quality filtered, and temporally filtered from June 01, 2020, to September 30, 2020. We did not filter the Sentinel-2 imagery; instead, to avoid cloudy data and minimize the impact of the tidal stage, the mean of the 60% to 80% range of data was used to target the high biomass period while minimizing cloud impacts.

2.4 Salt Marsh Extent

This study updates the NWI maps with a combination of Sentinel-1 and Sentinel-2 and an ensemble machine learning approach to predict the probability of a pixel being an emergent estuarine wetland. We used three machine learning algorithms (rotational forests, SVM, and XGBoost) in an ensemble approach. GEE was used to preprocess all remote sensing inputs.[46] Variables included Shuttle Radar Topography Mission (SRTM) (resampled to 10m), National Elevation Dataset, average Sentinel-1 VV, Sentinel-1 VH, all 10m Sentinel-2 bands (2, 3, 4, and 8), and NDVI and Normalized Difference Water Index. Mean values were calculated after filtering for cloud, quality, and temporally from June 01, 2020, to September 30, 2020.

Each model predicted the probability that a pixel within 1 km of NWI layers estuarine emergent class was salt marsh. We calculated the standard error of these probabilities and used that to predict a spatial estimate of extent uncertainty. We compared the performance of this uncertainty analysis with confidence intervals derived from the methods of Olofsson et al.[47]

Models were trained for individual watersheds or clusters of similar and spatially proximate watersheds. Approximately 5000 random points were placed within 1 km of salt marsh and designated salt marsh or not by the NWI. Using high-resolution imagery, we examined each salt marsh location to confirm that it was still a salt marsh in 2020. We used R statistical software (3.6.2) to train and classify each watershed area within 1 km of the NWI salt marsh boundary. These classifications were then post-processed, including merging areas smaller than three pixels within the marsh extent and requiring salt marsh to be within 100 m of salt marsh in the NWI. We conducted an accuracy assessment across the CONUS with a stratified random sample of 10,000 points.

2.5 Drivers of AGB in CONUS Salt Marsh

We explored spatial autocorrelation with Moran's I and Local Moran's I. Then, we utilized machine learning (XGBoost) and Shapley values to understand the relationship of AGB to drivers. Shapley values are a game theory approach to determining the variable contribution to a particular modeled outcome (Sundararajan and Najmi, 2020).[48] AGB was explored relative to potential drivers at a 3 km scale ($n = 8347$). Explanatory variables included PRISM climate data (August 2020 total precipitation and mean temperature);[49] average regional sea-level rise, tidal amplitude, and relative tidal elevation;[50] August 2020 composite of chlorophyll-a (NOAA/NESDIS/STAR 2022a);[51] August 2020 composite of diffuse attenuation coefficient (NOAA/NESDIS/STAR 2022b);[52] hurricane landfall and intensity;[53] C-CAP LCLU variables;[54] and water extent and change.[55] These variables represent likely drivers of biomass across the CONUS that are available at a <3 km^2 spatial resolution.

3 Results and Discussion

3.1 Model Comparison

The three machine learning algorithms' internal metrics performed similarly. For example, the out-of-bag (OOB) root mean square errors (RMSEs) were all within 100 $g\,m^{-2}$ (Table 1). The inclusion of Sentinel-1 and 2 had minimal impact on OOB metrics. However, we found a notable improvement in the RMSE of XGBoost over the other algorithms for the Georgia 2019 validation data at the site and vegetation plot scale. The Plum Island sampling extents were polygons (136 to 874 salt marsh pixels) with no exact sampling locations [Dataset];[41] therefore, we calculated a

Table 1 Machine learning model algorithm performance in both the OOB and validation datasets.

			Internal		Georgia		Plum Island, MA	
			OOB		Validation ($n = 158$)	Site validation ($n = 8$)	Validation type 1 ($n = 17$)	Validation type 2 ($n = 17$)
Algorithm	Training set	n	RMSE	R^2	RMSE	RMSE	RMSE	RMSE
Random Forest	Stable	723	**471.8**	0.54	325.0	196.07	561.8	452.0
	Complete	984	473.2	0.53	363.8	269.1	659.2	419.5
XGBoost	Stable	723	480.4	**0.54**	**301.0**	107.33	373.04	**221.5**
	Complete	984	474.1	0.50	326.1	194.2	**344.5**	232.3
SVM	Stable	723	489.2	0.52	304.0	**104.5**	372.4	308.5
	Complete	984	503.3	0.43	378.6	160.7	368.2	308.5
Landsat only XGBoost	Stable	723	481.1	0.52	368.5	179.9	374.3	237.2
	Complete	984	479.0	0.50	430.3	328.0	418.8	295.8

The best-performing metric is bolded in each category.

min, mean, and max values within the classified salt marsh extent for the location and compared, i.e., if a location had <500 g m^{-2} of biomass, we compared it with the minimum for that region, biomass between 500 and 1000 g m^{-2} was compared with the mean, and areas with greater than 1000 g m^{-2} were compared with the maximum of a region. XGBoost was the best-performing algorithm across the board and consistently performed better with the stable training data set. The models trained with only Landsat data performed worse in most metrics and were limited to a 30 m resolution. Therefore, we used XGBoost with Sentinel-1/2 to classify AGB for salt marsh areas across the CONUS. These results demonstrate similar uncertainty to other machine learning approaches in salt marsh environments, e.g., Chen et al.[56] found an RMSE of 371 g m^2 when predicting *Spartina alterniflora*.

Spatial variables (x and y), Landsat band 6, and Sentinel-1 VH polarization were the model's four most important variables (Fig. 7). Sentinel-2 NIR and NDVI were the ninth and eleventh most important variables, respectively. Although the 10 m models performed better compared with the 30 m results (Table 1), the Landsat inputs comprised 6 of the 10 most important variables, suggesting that relying on the Sentinel data alone would result in a loss of predictive power. The importance of Landsat bands is probably due to the time between *in situ* and Sentinel data collection.

3.2 Extent Classification

We estimated a CONUS salt marsh extent of 14,491 km^2. We found an overall accuracy of 96.34%. Following the methods of Olofsson et al.,[47] we determined a confidence interval of 3175.6 km^2, slightly less than the confidence interval derived from our machine learning approach (3473.5 km^2). These results suggest the multiple machine learning algorithm approach to be a reasonable estimate of error and useful for providing the locational uncertainty, which can result in a more precise understanding of AGB. The difference between the spatially derived upper and lower confidence intervals is evident when examined visually (Fig. 3). The most prominent differences between the low and high extents were the inclusion of similar ecosystems such as tidal mudflats and upland areas of possible salt marsh transition. In many areas, these differences were minor but represent 26% of the average estimate of biomass in the CONUS.

3.3 AGB Across the CONUS

The patterns of AGB varied significantly across the CONUS, including within individual watersheds. In the CONUS, a max AGB of 1735 g m^{-2} was found in HUC6 180701 (Ventura-San

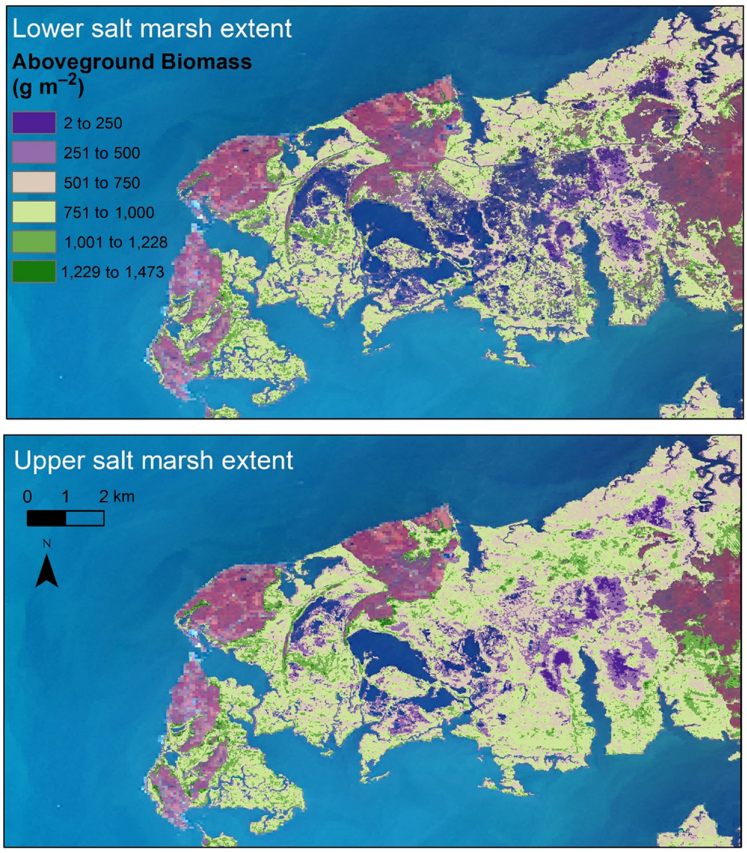

Fig. 3 Difference between the upper and longer spatial estimates of salt marsh extent. The upper extent includes all areas within the lower extent. Sentinel-2 imagery (NIR, G, B) in the background for a section of Deal Island, Maryland.

Gabriel Coast). In total, the CONUS had 8.32 (7.15 to 9.35) Tg of AGB in 2020, which using the conversion of 0.441 from Byrd et al.[18] would be 3.67 (3.15 to 4.12) Tg C. The upper salt marsh extent increased AGB slightly less than the lower extent decreased it. This reflects the inclusion of more low biomass areas in the upper salt marsh extent such as pixels with a mosaic of vegetation and unvegetated areas or tidal flats (Fig. 3). In comparison the entirety of North America's grasslands is estimated at 207.72 Tg C and an average of 75 $\mathrm{g\,C\,m^{-2}}$[57] compared with an average of 255.7 $\mathrm{g\,C\,m^{-2}}$ in salt marshes. Our average is significantly lower than global estimates from the literature (430 $\mathrm{g\,C\,m^{-2}}$) but very similar to the median value of 240 $\mathrm{g\,C\,m^{-2}}$[22]. This is due in part to not every $\mathrm{m^2}$ within a pixel being vegetated. Recent studies modeling gross primary production across tidal marshes of the CONUS found significantly higher productivity (4.32 ± 2.45 $\mathrm{g\,C/m^2/day}$[58]); this measure includes woody vegetation, the inclusion of pixels with high coverage, and coarser spatial resolution. Visually, biomass followed many expected trends when aggregated to 3×3 km areas, with low marsh areas having lower biomass and high marsh areas having slightly higher biomass (Fig. 4). These patterns were further explored within our explanatory machine learning analysis.

We compared the annual variation with the extent of uncertainty for a single year. These variables are expected to have a significant impact on AGB estimates, but how great an impact is unclear. We estimate their effect on the Lower Chesapeake Bay Watershed. The extent of uncertainty results in a range of 0.34 to 0.604 Tg of AGB in the watershed. In comparison, if the extent midpoint is used, the range of annual variation (2015 to 2020) was between 0.48 and 0.70 Tg of AGB. If the NWI extent is utilized, a very similar total AGB to the upper extent is estimated (0.607 Tg of AGB). Annual variation had a slightly larger effect on AGB uncertainty than the extent did, and we further explore the environmental variables that determine this variation with our machine learning analysis.

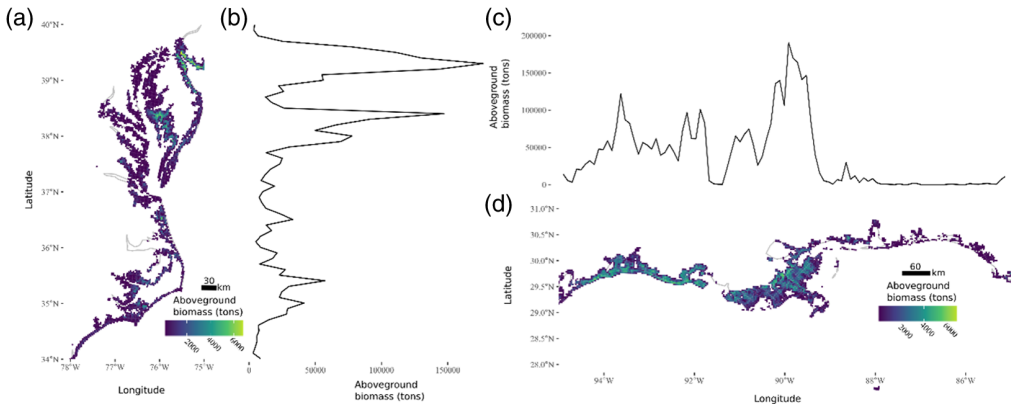

Fig. 4 (a) AGB for the Mid-Atlantic, USA, summed for the maximum extent of salt marsh within a 3×3 km area. (b) Latitudinal plot of total AGB summed for each 0.1 decimal degree. (c) AGB for the Gulf of Mexico, USA, summed for the maximum extent of salt marsh within a 3×3 km area. (d) Longitudinal plot of total AGB summed for each 0.1 decimal degree. Figure 8 is a CONUS-wide map.

CONUS-wide median biomass in 3×3 km bins with at least 20 pixels varied between a max of 1227.2 and a min of 38.4 occurring in HUC 6 watershed 020700 and 030902, respectively [Fig. 5(a)]. The Gulf of Mexico, Mid-Atlantic, and San Francisco Bay all had high median estimates of AGB. A pattern of increased AGB as you move inland is noticeable in the Mississippi

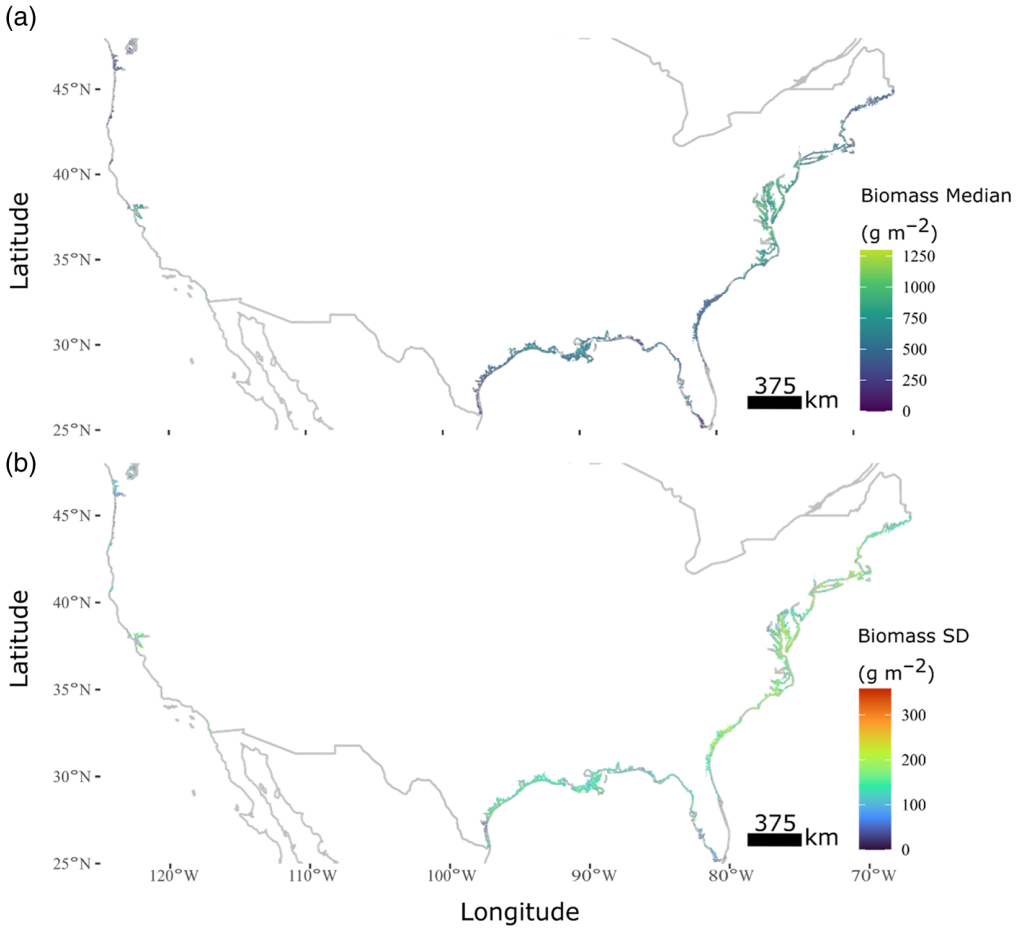

Fig. 5 (a) The median biomass across the CONUS and (b) the standard deviation across the CONUS. The 3×3 km squares had the median and standard deviation of all AGB estimates calculated.

Delta, suggesting that the increased AGB seen in Fig. 4 is due to both extent and AGB increases [Fig. 4(b)]. In the Chesapeake Bay, an increase in median AGB is evident in the fresher tributaries potentially due to *Phragmites australis*, which can have significantly more biomass than more salt-tolerant species such as *Spartina patens*.[59] The standard deviation was consistent across much of the CONUS with low AGB regions such as Georgia, southern Florida, Maine, Pacific Northwest, and Texas having lower standard deviations [Fig. 5(b)].

3.3.1 *Biomass drivers*

We found significant spatial autocorrelation of AGB using Moran's I ($I = 0.84$, $p < 0.001$). AGB clustering is expected due to climatic and tidal effects on AGB. Continuing our analysis of drivers, the four variables with the highest absolute Shapley value were tidal amplitude, relative sea level rise (RSLR), precipitation, and temperature (Fig. 6, Table 2). These impactful variables were split evenly between tidal/elevation and climate drivers. The drivers varied by region; e.g., hurricane landfall/category was the fifth most impactful variable in the Gulf Coast region. The response curves of the elevation drivers fit expectations with low rates of RSLR, which has limited or even negative effects on AGB and increases to a plateau. By contrast, high rates of RSLR (>5 mm year^{-1}) had a large negative effect on AGB. The response of AGB to tidal amplitude was interesting, with nontidal systems having lower biomass and a slight increase in microtidal systems. Then, AGB declined as amplitude increased [Fig. 6(d)]. This response is likely due to the greater range of vegetated tidal elevations in these high tidal amplitude systems and the greater likelihood of inundated pixels impacting the analysis. The response of AGB to precipitation fits the expectation, with low monthly precipitation reducing AGB. Drought is a major driver of salt marsh die-off.[60] By contrast, the relationship to temperature was more complicated, with AGB increasing to an inflection point around 26°C, which corresponds with approximately Cape Fear, South Carolina, coinciding with the upper extent of hurricane impacts in 2020.

In situ studies have examined climate drivers of AGB in salt marshes, including for a single species,[61] long-term spatio-temporal trends (Bice et al. 2023),[62] and latitudinal gradients of AGB's relationship to belowground biomass (BGB).[63] River discharge was found to be a major driver of *Spartina alterniflora* AGB, especially along creek banks.[61] Our study found precipitation to be a major driver, which is the closest analog to discharge in our set of drivers. A spatiotemporal analysis of AGB in a single watershed found temperature, river discharge, drought, sea level, and river nutrient concentrations to drive AGB (Biçe et al.). Precipitation was the only variable that was not found to have a causal link to AGB (Bice et al.). Our study did not have discharge data, river nutrient concentrations, or draught indicators, which likely have high covariance with precipitation. When a latitudinal analysis of the ratio of AGB to BGB was conducted

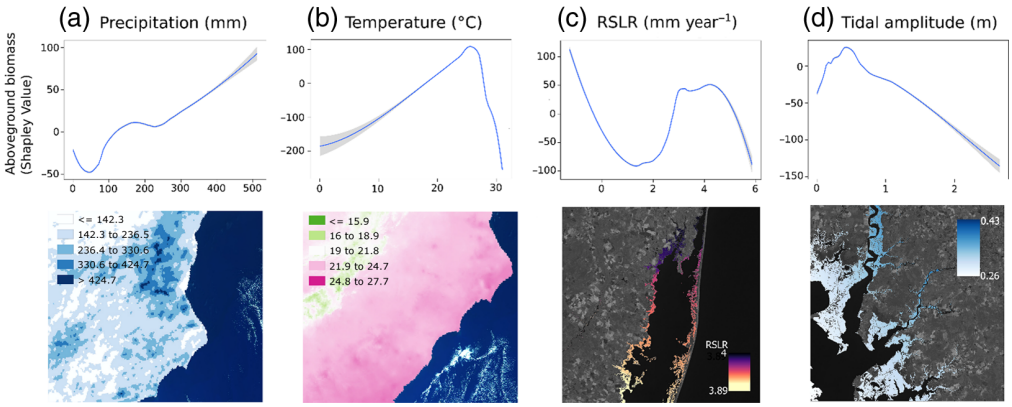

Fig. 6 Four most impactful drivers of AGB across the CONUS with examples of their spatial variation. Response curves demonstrate the average response of AGB to the variable at a certain value. (a) Precipitation visualized for a region of the Atlantic coast, (b) temperature for a region of the southern Atlantic coast, (c) RSLR for a section of the eastern shore of Maryland, and (d) tidal amplitude visualized for a region of Chesapeake Bay.

on the Atlantic Coast, trends in the increased allocation of BGB with lower temperatures were observed.[63] Our study does observe similar declines in AGB going from South Carolina to Massachusetts. However, Crosby et al.[63] only examined *Spartina alterniflora's* latitudinal response. These studies lack our study's large geographic scope but demonstrate similar trends, such as increased biomass as temperature increases.

The most significant variables did vary by coast. For example, the hurricane category was most impactful in the Gulf because that region had direct landfalls. Low precipitation likely explains the lower-than-expected AGB across the Gulf for 2020. The regional exploration of drivers allows for identifying climatic, tidal, and LCLU patterns that affect salt marsh biomass. Understanding current AGB and its drivers is critical for improving ecosystem resilience and change estimates.

AGB is a minor component of the larger salt marsh carbon budget, i.e., the mean carbon density of soil organic carbon (SOC) of salt marshes in the CONUS is 27.0 kg C m^{-3}. Still, SOC stock loss is more likely in marshes with low or no AGB.[64] This product's 10 m spatial resolution allows for finer scale determination of these loss areas. Repeat extent classification and AGB prediction can enable improved carbon monitoring. Future research directions should include global AGB prediction in tidal marsh ecosystems and assessment of regional trends in AGB at a 30 m spatial resolution.

This dataset has several limitations, including the focus on a singular blue carbon ecosystem, which ignores some of the complexity of coastal ecosystems and the gradient across these landscapes. The tidal filtering is limited in this approach and could be improved by incorporating algorithms with potential applications on Sentinel-2 data, such as Flooding in Landsat Across Tidal Systems.[65] Applications that require a high temporal resolution, such as monitoring the seasonality, would benefit from products such as Harmonized Landsat Sentinel-2[66] with little loss of information from the 30 m spatial resolution. AGB represents a small portion of the total carbon within these ecosystems, and individual pixels demonstrate high uncertainty when evaluating the test datasets. Using multiple sensors compounded the potential geolocation error and tidal stage impacts, which is one reason that uncertainty was reduced at the site level.

4 Conclusion

The proliferation of satellite data has led to an imbalance between remote sensing data and *in situ* data for training and validation. This work evaluated the use of *in situ* data with temporally noncoincident remote sensing data to address the mapping of salt marsh AGB at 10 m across the CONUS. Our CONUS-wide map of AGB demonstrates the current extent of salt marshes, AGB, and an estimate of aboveground carbon. The explanatory machine learning analysis demonstrates that the major drivers of AGB are RSLR, temperature, precipitation, and tidal amplitude. RSLR, temperature, and precipitation are forecasted to change significantly due to climate change, and as such, the future AGB of these ecosystems will change, potentially leading to more vulnerable coasts. Increases in temperature and RSLR rates could result in temporary increases in ABG in these ecosystems. However, continued increases in these drivers will result in a loss of ABG (Fig. 6). These results identify future conditions that will impact salt marsh health, including low AGB in drought conditions, high-temperature environments, and high rates of RSLR. Salt marsh AGB is an important carbon stock in the CONUS and an indicator of this ecosystem's much larger SOC stock. Remote sensing monitoring can provide a comprehensive understanding of the location and spatial variability, providing information for carbon monitoring and restoration.

5 Appendix

Model performance was evaluated with variable importance (Fig. 7), identifying location as the two most important variables. Patterns of AGB across the entire CONUS (Fig. 8) were further explored by using Shapley values to identify relationships between potential drivers and AGB (Table 2).

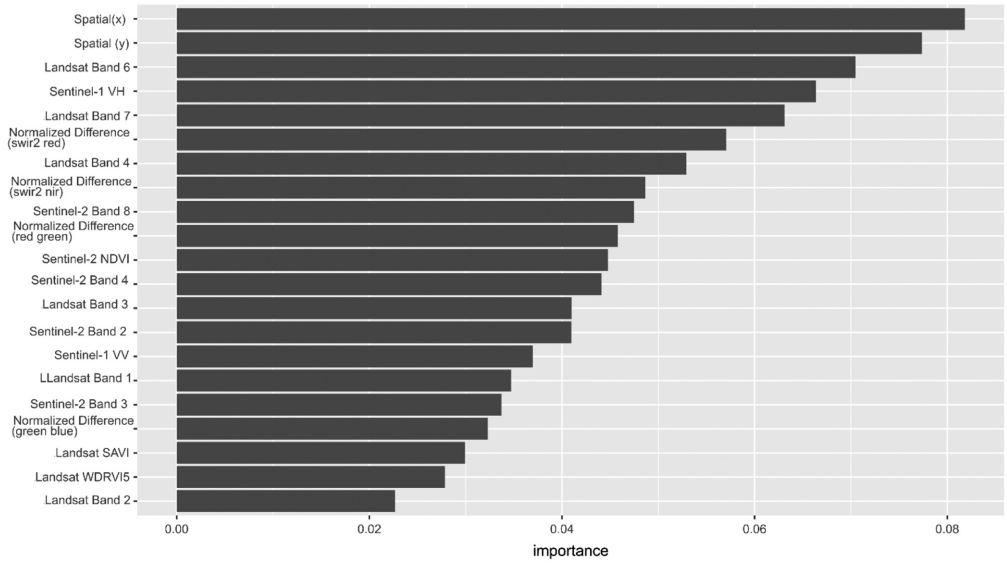

Fig. 7 Variable importance results for the best performing model (stable 10 m XGBoost).

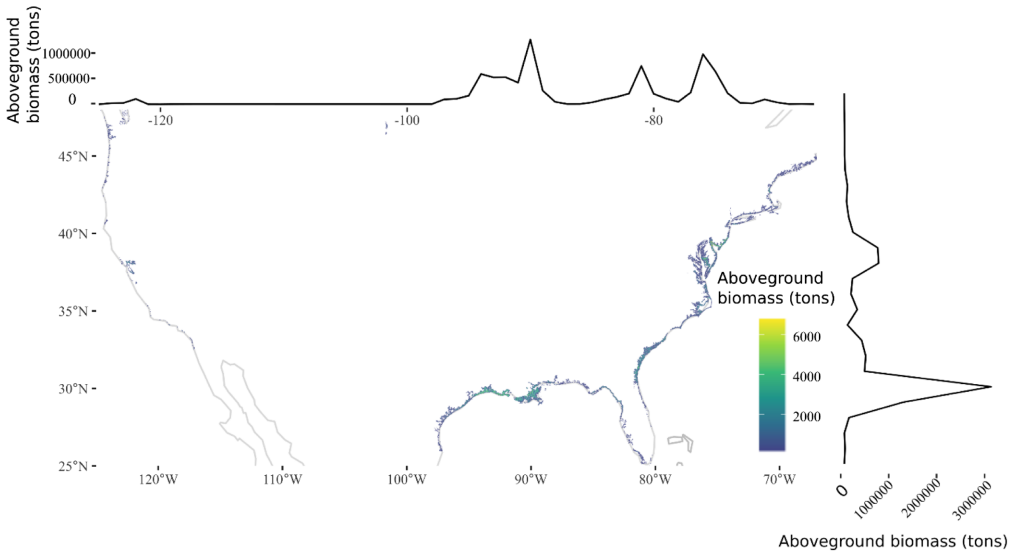

Fig. 8 Conus wide map of aboveground biomass and salt marsh extent in tons. 3×3 km squares had the total biomass within estimated and then summed by 0.1 decimal degrees to create the line plot.

Table 2 Shapley values for each predictor by coast (Gulf, East, and West).

Source	Feature	Units	East	Gulf	West
Holmquist and Windham-Myers 2021	Relative sea level rise	mm year^{-1}	68.43407	41.69719	61.49072
	Relative tidal elevation (m)	m	4.508742	7.696512	9.315143
	Low marsh	Landsat pixel	10.74071	3.876938	8.285119
	Tidal amplitude	m	12.48423	11.68048	29.7753
PRISM	Average August precipitation	in.	25.11258	41.91823	35.47062
	Average August temperature	C	47.45728	15.17227	65.24272
NOAA CoastWatch	Chlorophyll-a	mg m^{-3}	6.477258	4.69026	4.72075
	Diffuse attenuation coefficient	m^{-1}	11.67757	5.376114	15.04863

Table 2 (*Continued*).

Source	Feature	Units	East	Gulf	West
HURDAT	Intensity	Category	0.407281	20.49156	0
	HURIN19	Hurricane landfall	9.16118	0.27083	0
NOAA C-CAP 2016	High developed	Landsat pixel	3.499407	1.781245	6.070576
	Medium developed	Landsat pixel	6.759439	4.263299	13.82716
	Low developed	Landsat pixel	8.384758	8.136608	8.08088
	Cropland	Landsat pixel	6.223649	1.055741	3.504637
	Hay	Landsat pixel	1.050245	1.068626	7.03032
	Palustrine forest wetland	Landsat pixel	6.849268	7.566241	3.133879
	Palustrine scrub-shrub wetland	Landsat pixel	7.07663	3.697094	9.687406
	Palustrine emergent wetland	Landsat pixel	5.484677	4.545797	7.635535
	Estuarine forest wetland	Landsat pixel	1.353277	10.99697	1.436495
	Estuarine scrub-shrub wetland	Landsat pixel	6.282705	3.853517	5.721189
	Estuarine emergent wetland	Landsat pixel	7.100773	11.97486	12.23928
	Unconsolidated Shore	Landsat pixel	6.327699	5.190106	15.27066
	Water	Landsat pixel	7.479439	7.099599	6.006875
Sentinel-2 Water	Seasonal	Landsat pixel	13.80347	9.01653	11.31441
	New seasonal	Landsat pixel	10.04823	6.077725	9.022613
	Lost seasonal	Landsat pixel	4.308007	8.474712	5.353308
	Seasonal to Permanent	Landsat pixel	5.940834	5.694759	5.842455
	Ephemeral Permanent	Landsat pixel	3.771946	3.747837	2.843304
	Seasonal	Landsat pixel	1.376247	1.404641	5.414144

Shapley values are the absolute mean values for each of the predictors.

Code and Data Availability

Classification and regression code can be found on GitHub: https://github.com/campban/biomass_sm/. Data products are available at https://doi.org/10.3334/ORNLDAAC/2348. Sentinel-2 data can be accessed at https://sentinel.esa.int/web/sentinel/user-guides/sentinel-2-msi/processing-levels/level-2, and Landsat data can be accessed at https://www.usgs.gov/landsat-missions/landsat-data-access.

Acknowledgments

This research was supported in part by the NASA Carbon Monitoring System program (Grant No. 16-CMS16-0073). A.D.C. was supported by the NASA Postdoctoral Program Fellowship administered by Oak Ridge Associated Universities.

References

1. O. Hoegh-Guldberg, E. Northrop, and J. Lubchenco, "The ocean is key to achieving climate and societal goals," *Science* **365**, 1372–1374 (2019).
2. J. R. Holmquist et al., "Uncertainty in United States coastal wetland greenhouse gas inventorying," *Environ. Res. Lett.* **13**, 115005 (2018).
3. A. L. Hinson, R. A. Feagin, and M. Eriksson, "Environmental controls on the distribution of tidal wetland soil organic carbon in the continental United States," *Glob. Biogeochem. Cycles* **33**, 1408–1422 (2019).

4. A. L. Hinson et al., "The spatial distribution of soil organic carbon in tidal wetland soils of the continental United States," *Glob. Change Biol.* **23**, 5468–5480 (2017).
5. D. M. Alongi, "Carbon balance in salt marsh and mangrove ecosystems: a global synthesis," *J. Mar. Sci. Eng.* **8**(10), 767 (2020).
6. E. Mcleod et al., "A blueprint for blue carbon: toward an improved understanding of the role of vegetated coastal habitats in sequestering CO_2," *Front. Ecol. Environ.* **9**(10), 552–560 (2011).
7. D. Herr and E. Landis, *Coastal blue carbon ecosystems. Opportunities for nationally determined contributions*, Policy Brief, IUCN, Gland, Switzerland and TNC, Washington, DC, USA (2016).
8. A. D. Campbell et al., "Global hotspots of salt marsh change and carbon emissions," *Nature* **612**(7941), 701–706 (2022).
9. M. Schuerch et al., "Future response of global coastal wetlands to sea-level rise," *Nature* **561**, 231–234 (2018).
10. D. M. FitzGerald et al., "Largest marsh in New England near a precipice," *Geomorphology* **379**, 107625 (2021).
11. N. W. Schieder, D. C. Walters, and M. L. Kirwan, "Massive upland to wetland conversion compensated for historical marsh loss in Chesapeake Bay, USA," *Estuaries Coasts* **41**, 940–951 (2018).
12. C. R. Field, C. Gjerdrum, and C. S. Elphick, "Forest resistance to sea-level rise prevents landward migration of tidal marsh," *Biol. Conserv.* **201**, 363–369 (2016).
13. J. R. Holmquist, L. N. Brown, and G. M. MacDonald, "Localized scenarios and latitudinal patterns of vertical and lateral resilience of tidal marshes to sea-level rise in the contiguous United States," *Earth's Future* **9**(6), e2020EF001804 (2021).
14. L. S. Smart et al., "Aboveground carbon loss associated with the spread of ghost forests as sea levels rise," *Environ. Res. Lett.* **15**, 104028 (2020).
15. M. F. Gross, V. Klemas, and J. E. Levasseur, "Remote sensing of Spartina anglica biomass in five French salt marshes," *Int. J. Remote Sens.* **7**, 657–664 (1986).
16. M. F. Gross et al., "Quantification of biomass of the marsh grass *Spartina alterniflora* Loisel using Landsat Thematic Mapper imagery," *Photogramm. Eng. Remote Sens.* **53**, 1577–1583 (1987).
17. M. A. Hardisky et al., "Remote sensing of biomass and annual net aerial primary productivity of a salt marsh," *Remote Sens. Environ.* **16**, 91–106 (1984).
18. K. B. Byrd et al., *Aboveground biomass high-resolution maps for selected US tidal marshes, 2015*, ORNL DAAC (2018).
19. K. B. Byrd et al., "Evaluation of sensor types and environmental controls on mapping biomass of coastal marsh emergent vegetation," *Remote Sens. Environ.* **149**, 166–180 (2014).
20. C. L. Doughty and K. C. Cavanaugh, "Mapping coastal wetland biomass from high resolution unmanned aerial vehicle (UAV) imagery," *Remote Sens.* **11**(5), 540 (2019).
21. D. Jensen et al., "Aboveground biomass distributions and vegetation composition changes in Louisiana's Wax Lake Delta," *Estuarine Coast. Shelf Sci.* **250**, 107139 (2021).
22. K. B. Byrd et al., "Corrigendum to 'A remote sensing-based model of tidal marsh aboveground carbon stocks for the conterminous United States' [ISPRS J. Photogram. Rem. Sens. 139 (2018) 255-271]," *ISPRS J. Photogramm. Remote Sens.* **166**, 63–67 (2020).
23. C. Li, L. Zhou, and W. Xu, "Estimating aboveground biomass using Sentinel-2 MSI data and ensemble algorithms for grassland in the Shengjin Lake Wetland, China," *Remote Sens.* **13**, 1595 (2021).
24. S. Sun et al., "Modelling aboveground biomass carbon stock of the Bohai Rim coastal wetlands by integrating remote sensing, terrain, and climate data," *Remote Sens.* **13**(21), 4321 (2021).
25. A. D. Campbell and Y. Wang, "Salt marsh monitoring along the mid-Atlantic coast by Google Earth Engine enabled time series," *PloS One* **15**(2), e0229605 (2020).
26. V. L. Woltz et al., "Above- and belowground biomass carbon stock and net primary productivity maps for tidal herbaceous marshes of the United States," *Remote Sens.* **15**(6), 1697 (2023).
27. T. E. Dahl and S. M. Stedman, *Status and trends of wetlands in the coastal watersheds of the conterminous United States 2004 to 2009* (2013).
28. E. Gage, D. J. Cooper, and R. Lichvar, "Comparison of USACE three-factor wetland delineations to national wetland inventory maps," *Wetlands* **40**, 1097–1105 (2020).
29. T. D. Pham et al., "Advances in Earth observation and machine learning for quantifying blue carbon," *Earth-Sci. Rev.* **243**, 104501 (2023).
30. L. Breiman, "Random forests," *Mach. Learn.* **45**, 5–32 (2001).
31. L. Goldberg et al., "Global declines in human-driven mangrove loss," *Glob. Change Biol.* **26**(10), 5844–5855 (2020).
32. O. Mutanga, E. Adam, and M. A. Cho, "High density biomass estimation for wetland vegetation using WorldView-2 imagery and random forest regression algorithm," *Int. J. Appl. Earth Observ. Geoinf.* **18**, 399–406 (2012).
33. Y. Li et al., "Forest aboveground biomass estimation using Landsat 8 and Sentinel-1A data with machine learning algorithms," *Sci. Rep.* **10**(1), 9952 (2020).

34. V. Vapnik, *The Nature of Statistical Learning Theory*, Springer Science & Business Media (2013).
35. N. Thomas et al., "High-resolution mapping of biomass and distribution of marsh and forested wetlands in southeastern coastal Louisiana," *Int. J. Appl. Earth Observ. Geoinf.* **80**, 257–267 (2019).
36. T. A. Worthington et al., "The distribution of global tidal marshes from earth observation data," *Glob. Ecol. Biogeogr.* **33**(8), e13852 (2024).
37. S. C. Pennings and M. D. Bertness, "Salt marsh communities," in *Marine Community Ecology*, M. D. Bertness, S. D. Gaines, and M. Hay, Eds., pp. 289–316, Sinauer Associates, Sunderland (2001).
38. K. D. Bromberg and M. D. Bertness, "Reconstructing New England salt marsh losses using historical maps," *Estuaries* **28**, 823–832 (2005).
39. B. Bischl et al., "mlr: Machine Learning in R.," *J. Mach. Learn. Research* **17**(170), 1–5 (2016).
40. Georgia Coastal Ecosystems LTER Project andS. C. Pennings, "Fall 2019 plant monitoring survey – biomass calculated from shoot height and flowering status of plants in permanent plots at GCE sampling sites 1–10 ver 9," Environmental Data Initiative (2021). https://doi.org/10.6073/pasta/9418b615a46715305e14bffd9ccde40d.
41. J. Byrnes, "PIE LTER plant biomass associated with marsh sites used in space for time sea level rise study, Rowley, MA. ver 2," Environmental Data Initiative (2020). https://doi.org/10.6073/pasta/895e4278b794533c94d3b3eee2211c93 (accessed 29 November 2021).
42. J. T. Morris, K. Sundberg, and C. S. Hopkinson, "Salt marsh primary production and its responses to relative sea level and nutrients in estuaries at Plum Island, Massachusetts, and North Inlet, South Carolina, USA," *Oceanography* **26**, 78–84 (2013).
43. S. J. Taylor and B. Letham, "Forecasting at scale," *Am. Statistician* **72**(1), 37–45 (2018).
44. C. Campbell et al., "*Net primary production and standing biomass in northern continental wetlands*," Information Report-Northern Forestry Centre, Canadian Forest Service (2000).
45. J. L. O'Connell et al., "The Tidal Marsh Inundation Index (TMII): an inundation filter to flag flooded pixels and improve MODIS tidal marsh vegetation time-series analysis," *Remote Sens. Environ.* **201**, 34–46 (2017).
46. E. R. DeLancey et al., "Monitoring hydro temporal variability in Alberta, Canada with multi-temporal Sentinel-1 SAR data," *Can. J. Remote Sens.* **44**(1), 1–10 (2018).
47. P. Olofsson et al., "Good practices for estimating area and assessing accuracy of land change," *Remote Sens. Environ.* **148**, 42–57 (2014).
48. M. Sundararajan and A. Najmi, "The many Shapley values for model explanation," in *Int. Conf. Mach. Learn.*, pp. 9269–9278 (2020).
49. PRISM Climate Group, Oregon State University, (data created 4 Feb 2014). https://prism.oregonstate.edu (accessed 1 August 2022).
50. J. R. Holmquist and L. Windham-Myers, *Relative tidal marsh elevation maps with uncertainty for conterminous USA, 2010*, ORNL DAAC, Oak Ridge, Tennessee, USA (2021).
51. NOAA/NESDIS/STAR, 2022.a Chlorophyll Concentration, OC3 Algorithm, Version 1.3. NOAA CoastWatch, National Centers for Environmental Information (NCEI), https://coastwatch.noaa.gov, https://www.ncei.noaa.gov/ (accessed 1 January 2022).
52. NOAA/NESDIS/STAR, 2022.b Diffuse Attenuation Coefficient at 490 nm. Version 1.3, NOAA CoastWatch, National Centers for Environmental Information (NCEI), https://coastwatch.noaa.gov, https://www.ncei.noaa.gov/ (accessed 1 January 2022).
53. C. W. Landsea and J. L. Franklin, "Atlantic hurricane database uncertainty and presentation of a new database format," *Mon. Weather Rev.* **141**, 3576–3592 (2013).
54. J. E. Dobson, "NOAA coastal change analysis program (CCAP)," NOAA Tech. Rep. NMFS, p. 123 (1995).
55. J. F. Pekel et al., "High-resolution mapping of global surface water and its long-term changes," *Nature* **540**(7633), 418–422 (2016).
56. C. Chen et al., "Aboveground biomass of salt-marsh vegetation in coastal wetlands: sample expansion of in situ hyperspectral and Sentinel-2 data using a generative adversarial network," *Remote Sens. Environ.* **270**, 112885 (2022).
57. J. Xia et al., "Spatio-temporal patterns and climate variables controlling of biomass carbon stock of global grassland ecosystems from 1982 to 2006," *Remote Sens.* **6**, 1783–1802 (2014).
58. R. A. Feagin et al., "Tidal wetland gross primary production across the continental United States, 2000–2019," *Glob. Biogeochem. Cycles* **34**, e2019GB006349 (2020).
59. L. Windham, "Comparison of biomass production and decomposition between Phragmites australis (common reed) and Spartina patens (salt hay grass) in brackish tidal marshes of New Jersey, USA," *Wetlands* **21**(2), 179–188 (2001).
60. M. Alber et al., "Salt marsh dieback: an overview of recent events in the US," *Estuarine, Coastal Shelf Sci.* **80**(1), 1–11 (2008).
61. K. Więski and S. C. Pennings, "Climate drivers of *Spartina alterniflora* saltmarsh production in Georgia, USA," *Ecosystems* **17**, 473–484 (2014).

62. K. Biçe et al., "Temporal patterns and causal drivers of aboveground plant biomass in a coastal wetland: Insights from time-series analyses," *Frontiers in Marine Sci.* **10**, 1130958 (2023).
63. S. C. Crosby et al., "*Spartina alterniflora* biomass allocation and temperature: implications for salt marsh persistence with sea-level rise," *Estuaries Coasts* **40**, 213–223 (2017).
64. R. R. Lane et al., "Fate of soil organic carbon during wetland loss," *Wetlands* **36**, 1167–1181 (2016).
65. C. R. Narron et al., "Flooding in Landsat across tidal systems (FLATS): an index for intermittent tidal filtering and frequency detection in salt marsh environments," *Ecol. Indic.* **141**, 109045 (2022).
66. M. Claverie et al., "The harmonized Landsat and Sentinel-2 surface reflectance data set," *Remote Sens. Environ.* **219**, 145–161 (2018).

Anthony D. Campbell received his PhD in biological and environmental science from the University of Rhode Island. He is an assistant research scientist with Goddard Earth Sciences Technology and Research II at the University of Maryland, Baltimore County. His research interests include remote sensing of blue carbon, biodiversity, and all things coastal.

Lola Fatoyinbo received her PhD in environmental sciences with a focus on forest ecology and remote sensing of mangrove wetlands from the University of Virginia. She is a research scientist in the Biospheric Sciences Lab at NASA Goddard Space Flight Center. She is a member of the GEDI and ICESat-2 Mission Science Teams. Her research interests include forest ecology and ecosystem structure with remote sensing.